Tracing Atlantic Waters Using ^{129}I and ^{236}U in the Fram Strait in 2016

A.-M. Wefing[1,2] (ID), **M. Christl[1]** (ID), **C. Vockenhuber[1]**, **M. Rutgers van der Loeff[3]** (ID), **and N. Casacuberta[1,2]** (ID)

[1]Laboratory of Ion Beam Physics, ETH Zurich, Zurich, Switzerland, [2]Environmental Physics, Institute of Biogeochemistry and Pollutant Dynamics, ETH Zurich, Zurich, Switzerland, [3]Marine Geochemistry, Alfred Wegener Institute, Bremerhaven, Germany

Abstract In this study ^{129}I and ^{236}U concentrations in seawater samples collected onboard R/V Polarstern during the PS100 expedition in the Fram Strait in 2016 are presented. The overall aim of the study was to investigate the distribution of these long-lived radionuclides along the transect located at 79°N. The combination of both radionuclides was used for the first time in the Fram Strait to trace ocean circulation pathways of Atlantic waters. Results show that both ^{129}I and ^{236}U concentrations as well as ^{236}U/^{238}U ratios are about two times higher ($> 600 \times 10^7$ at kg$^{(-1)}$, $> 20 \times 10^6$ at kg$^{(-1)}$, and 2.8×10^{-9}, respectively) in the cold and fresh outflowing surface waters from the Arctic Ocean (Polar Surface Water, PSW) compared to inflowing Atlantic origin waters (300×10^7 at kg$^{(-1)}$ ^{129}I, 12×10^6 at kg$^{(-1)}$ ^{236}U, and 1.4×10^{-9} ^{236}U/^{238}U). A comparison with the different ^{129}I and ^{236}U input functions for the Atlantic branches entering the Arctic Ocean reveals that the middepth Atlantic origin waters outflowing the Arctic Ocean show more influence of the Barents Sea Branch Water than the Fram Strait Branch Water. The high radionuclide concentrations observed in the PSW indicate substantial influence of the Norwegian Coastal Current. This current carries a significantly larger proportion of ^{129}I and ^{236}U releases from European reprocessing plants than the aforementioned Atlantic branches. We estimate surface water transit times from the northern Norwegian Coast through the Arctic to the PSW of 12–19 years, less than for the middepth Barents Sea Branch Water (16–23 years).

Plain Language Summary In this work we reconstructed the circulation of Atlantic waters in- and outflowing the Arctic Ocean through one of the main gates connecting these two oceans: the Fram Strait, located between Greenland and Svalbard. We measured the long-lived artificial radionuclides ^{129}I and ^{236}U to track the different water masses. These two radionuclides are present in the marine environment after the nuclear weapon tests (1950s-1960s) and from two European nuclear reprocessing plants (from 1960's until today). In particular the input of ^{129}I from these two reprocessing plants changed over time and can therefore also be used to estimate travel times of water masses. We collected 140 seawater samples at various depths from the Fram Strait in summer 2016. Our results depict higher concentrations of ^{129}I and ^{236}U in the waters outflowing the Arctic Ocean compared to those entering the polar region through the Fram Strait. The combination of ^{129}I and ^{236}U allowed us to distinguish between three main branches of Atlantic origin waters outflowing the Arctic Ocean having different travel times through the Arctic Ocean. We proved that ^{129}I and ^{236}U have a great potential as tracers to understand ocean circulation and travel times in the Arctic and North Atlantic oceans.

1. Introduction

Oceanographic processes in the Arctic Ocean and the Nordic Seas affect the world ocean circulation especially via their influence on deep-water formation within the Atlantic meridional overturning circulation (AMOC; e.g., Carmack & Aagaard, 1973; Killworth, 1983; Rudels, 1995; Tanhua et al., 2005). The main gateway and only opening allowing for deep-water exchange down to 2,600 m between the Nordic Seas and the Arctic Ocean is the Fram Strait, located between Greenland and Svalbard. The transport of warm Atlantic waters into the Arctic Ocean and the southward transport of cold Arctic Waters both occur the Fram Strait (e.g., Beszczynska-Möller et al. 2011, and references therein). This exchange of water masses is of particular interest in the context of global warming and accompanying changes in the Arctic environment, as it has been recently suggested that the Atlantic waters are the main drivers for temperature increase and sea ice loss in the Arctic Ocean (Polyakov et al., 2005, 2017).

To study circulation patterns of Atlantic origin waters in the Nordic Seas and the Arctic Ocean, artificial (anthropogenic) radionuclides released from nuclear weapon tests and reprocessing plants (RPs) can be used as tracers (Hou, 2004; Kershaw & Baxter, 1995; Raisbeck et al., 1995). Among them, the long-lived radionuclide ^{129}I (half-life $T_{1/2} = 15.7$ Myr) and, in line with advances in measurement techniques, also ^{236}U ($T_{1/2} = 23.5$ My) are of particular interest due to their conservative nature in the open ocean (e.g., Alfimov et al., 2013; Casacuberta et al., 2018, 2016; Smith et al., 2011). ^{129}I and ^{236}U have been released in significant amounts (6,000 kg and about 100 kg to date, respectively) by the two European RPs located in Sellafield (Great Britain) and La Hague (France; Figure S1). The releases from Sellafield are transported around the northern coast of Scotland and partly enter the North Sea between the Scottish coast and the Shetland Islands, whereas the La Hague releases are almost completely transported eastward, entering the North Sea via the English Channel. North Sea waters tagged with ^{129}I and ^{236}U are subsequently transported northward by the Norwegian Coastal Current (NCC; Figure 1a; Christl, Casacuberta, Vockenhuber, et al., 2015; Edmonds et al., 2001; Smith et al., 2011; Gascard et al., 2004). They further mix with waters of North Atlantic origin carrying the tracer signal of nuclear weapon tests, referred to as global fallout (GF; in total about 90 kg of ^{129}I; Snyder et al., 2010, and 900 kg of ^{236}U; Sakaguchi et al., 2009), and the combined tracer signal then enters the Arctic Ocean either via the Fram Strait (through the Fram Strait Branch Water [FSBW]) or via the Barents Sea (Barents Sea Branch Water [BSBW]). Overall, about 90% of the measured ^{236}U has been introduced by GF and about 10% by RP, whereas ^{129}I is almost exclusively assigned to RP releases (98%). RP releases of ^{129}I and ^{236}U varied with time, leading to an overall increasing input function for the ^{129}I/^{236}U atom ratio (Figure S1c).

Apart from the temporal variation of ^{129}I/^{236}U from RP, the combination of ^{129}I and ^{236}U allows distinguishing between the two main anthropogenic sources (i.e., RP and GF), as they are characterized by very different ^{129}I and ^{236}U concentrations as well as ^{129}I/^{236}U atom ratios (Casacuberta et al., 2018, 2016). To this purpose, the dual-tracer approach of using the ^{236}U/^{238}U ratio together with the ^{129}I/^{236}U ratio has been suggested and used to constrain sources of water masses (Christl, Casacuberta, Vockenhuber, et al., 2015; Casacuberta et al., 2016).

Multiple studies have examined the ^{129}I distribution in the Arctic Ocean, the Nordic Seas, and the North Atlantic Ocean (Aldahan et al., 2007; Alfimov et al., 2013, Alfimov, Aldahan, & Possnert, 2004, Alfimov, Aldahan, Possnert, Kekli, et al., 2004, Alfimov, Aldahan, Possnert, & Winsor, 2004; Buraglio et al., 1999; Edmonds et al., 1998; Gascard et al., 2004; Kilius et al., 1995; Smith et al., 1999, 1998), and the time-dependent input function has been used to calculate tracer ages of Atlantic waters as well as transit time distributions (Smith et al., 2005, 2011). ^{129}I transport and distribution in the North Atlantic and Arctic Ocean have also been subject to modeling approaches (Karcher et al., 2012; Orre et al., 2010). This is less the case for ^{236}U, which has only emerged as a new water mass tracer in recent years (Casacuberta et al., 2014; Castrillejo et al., 2017; Christl et al., 2017; Christl, Lachner, et al., 2013; Christl et al., 2012; Qiao et al., 2017; Sakaguchi et al., 2012, 2009; Steier et al., 2008). For the Fram Strait, so far only one study presented the ^{129}I distribution (Alfimov, Aldahan, & Possnert, 2004), while no ^{236}U data from this domain were available up to date.

In this work, we present ^{129}I and ^{236}U data from full depth profiles on a transect through the Fram Strait, collected during the PS100 expedition with R/V Polarstern in 2016 (Kanzow, 2017). The combination of both radionuclides in the dual-tracer approach allowed distinguishing between GF and RP influence in the different water masses flowing through the Fram Strait. ^{129}I and ^{236}U concentrations obtained for the outflowing waters in the Fram Strait indicate a large influence of NCC waters in the surface. Finally, we make use of the split input functions for ^{129}I defined recently (Casacuberta et al., 2018) to calculate transit times of waters transported from the Barents Sea through the Arctic Ocean to the Fram Strait by the different Atlantic branches.

2. Materials and Methods

2.1. Study Area

The Fram Strait is the largest gateway between the Nordic Seas and the Arctic Ocean, with a width of about 450 km and a sill depth of 2,600 m (Rudels et al., 2015). In the surface waters of the eastern part of the Fram
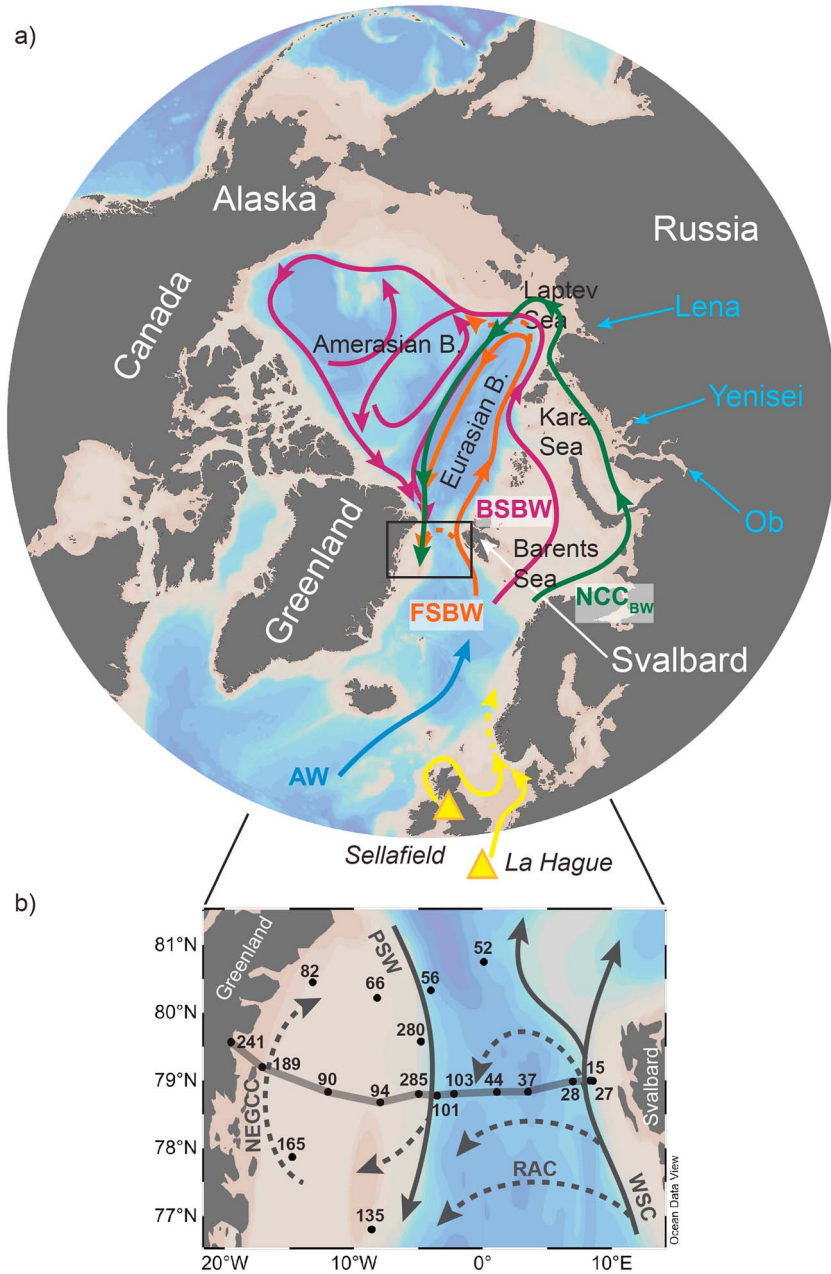
Figure 1. (a) Circulation scheme of Atlantic origin waters in the Arctic Ocean following Rudels (2009) and Rudels et al. (2004). Yellow represents branches from Sellafield and La Hague, orange represents Fram Strait Branch Water (FSBW), purple represents Barents Sea Branch Water (BSBW), and green represents Norwegian Coastal Current Branch Water (NCC$_{BW}$), AW: Atlantic Waters. The black rectangle depicts the study area shown in (b). (b) Fram Strait study area with surface currents and stations sampled for ^{129}I and ^{236}U analysis during the PS100 cruise in 2016 (in light gray: the transect shown in Figure 3). Return Atlantic Current (RAC) and North East Greenland Coastal Current (NEGCC) are represented in gray dashed arrows. PSW, Polar Surface Water; WSC, West Spitsbergen Current.

Strait, the West Spitsbergen Current (WSC) transports warm and saline Atlantic waters northward into the Arctic Ocean (Figure 1b). These waters are found down to a depth of about 500 m and partly represent waters that recirculated within the Fram Strait already (e.g., Beszczynska-Moller et al., 2012; Hattermann et al., 2016). The magnitude and exact location of this recirculation are still unclear and most probably also variable with time. North of Svalbard, the WSC turns eastward and the Atlantic origin waters enter the Arctic Ocean (Figure 1a, Rudels, 2009; Rudels et al., 2015). They move further eastward along the

Eurasian continental slope and a large portion of the former WSC waters presumably recirculates within the Nansen basin (Rudels, 2009). In the western part of the Fram Strait the cold and fresh surface waters exiting the Arctic Ocean are referred to as Polar Surface Water (PSW; Rudels et al., 2005), which is part of the southward flowing East Greenland Current (EGC). The core of the EGC is found along the shelf break of Greenland; however, it also partly spreads across the shelf, recirculates, and interacts with the local, northward flowing North East Greenland Coastal Current (NEGCC; Budéus et al., 1997; Figure 1b). In addition, the EGC waters on the shelf are influenced by melt waters from Greenland (Dodd et al., 2012, 2009; Stedmon et al., 2015). In the middle of the Fram Strait (around 0–5°W), the PSW spreads above the WSC due to its lower density and both water masses partly mix. Below the PSW and the WSC, the prevailing water masses in the Fram Strait are recirculated Arctic waters and intermediate and deep waters that are significantly colder than the WSC (Rudels et al., 2000; Schlichtholz & Houssais, 2002).

2.2. Seawater Sampling

Seawater samples presented in this study were collected during the R/V Polarstern expedition PS100 *GRIFF* from 18 July to 6 September 2016 (Kanzow, 2017) that was part of the international GEOTRACES program (www.bodc.ac.uk/geotraces/cruises/). The study area of this cruise comprised the Fram Strait between 76 and 81° N. For the analysis of ^{129}I and ^{236}U, 140 seawater samples were taken at 19 stations (full-depth profiles), of which 11 stations cover the 79°N transect from Svalbard to Greenland (Figure 1b). Samples were taken with twenty-four 12-L Niskin bottles mounted on a conductivity-temperature-depth rosette equipped with Sea-Bird sensors recording conductivity, temperature, and depth. For the analysis of ^{129}I, 200–500 ml of seawater is required that was directly filled into plastic bottles without any pretreatment. The ^{129}I chemical purification and preparation for the AMS measurement were carried out in the wet-labs on-board R/V Polarstern. About 3–5 L of unfiltered seawater was taken for ^{236}U analysis, and the preconcentration of Uranium was also carried out on-board. All samples were sent to ETH Zürich for further chemical treatment and final measurements using accelerator mass spectrometry (AMS).

2.3. ^{129}I Purification and AMS Measurement

The purification of ^{129}I carried out during the cruise followed the method described in Casacuberta et al. (2016), which is based on Michel et al. (2012). Briefly, the sample was adjusted to pH 6–7 and spiked with about 1.5 mg of Woodward Iodine ^{127}I. Iodine was purified using ion exchange columns filled with DOWEX 1×8 resin and directly precipitated as silver iodine (AgI). Dried precipitates were pressed into Ti targets before their measurement. All samples were measured at the Laboratory of Ion Beam Physics at ETH Zürich, using the compact 0.5 MV AMS system Tandy. The measurement routine is described in detail in Vockenhuber et al. (2015). Measured ^{129}I/^{127}I atom ratios were normalized using the in-house standard D22 with a nominal value of ^{129}I/^{127}I = $(50.35 \pm 1.61) \times 10^{-12}$ (Christl, Vockenhuber, et al., 2013). ^{129}I concentrations were calculated from the well-known amount of ^{127}I added as a spike. A replicate study using the different Woodward Iodine solutions resulted in an uncertainty of 2% that was taken as the uncertainty of the Woodward Iodine ^{127}I solution. Seawater samples were corrected for ^{129}I measured in chemistry blanks ($n = 11$) that were prepared with MilliQ water (18.2 MΩ high-purity water, Merck) onboard the research vessel. On average, $(1.29 \pm 0.27) \times 10^{6}$ atoms of ^{129}I were measured in the blanks, corresponding to a range of 1 to 10% of the total ^{129}I in seawater samples.

2.4. ^{236}U Purification and AMS Measurement

The preparation of samples for ^{236}U measurements followed the method of Casacuberta et al. (2016) and Castrillejo et al. (2017). Samples were collected in calibrated 3- to 5-L plastic bottles, acidified to pH 2 with concentrated HNO$_3$, and spiked with about 3pg ^{233}U (IRMM_051 spike). Uranium was preconcentrated by iron coprecipitation, adding about 200 mg of purified iron to the sample. In the laboratory facilities at Laboratory of Ion Beam Physics (ETH Zürich), the precipitates were dissolved and passed through prepacked ion exchange columns filled with Triskem UTEVA resin. U was precipitated again, dried down, and pressed into Ti targets before their measurement. The measurement routine for ^{236}U measurements is given in Christl, Casacuberta, Lachner, et al. (2015) and comprises measurements of ^{233}U/^{238}U and ^{236}U/^{238}U atom ratios. The U ratios are normalized to the ETH Zürich in-house standard ZUTRI with nominal isotopic ratios of $(4,055 \pm 203) \times 10^{-12}$ for ^{236}U/^{238}U and $(33,170 \pm 830) \times 10^{-12}$ for ^{233}U/^{238}U (Christl, Vockenhuber, et al., 2013). ^{236}U and ^{238}U concentrations were calculated from the known amount of ^{233}U

added as a spike. Seawater samples were corrected for ^{236}U measured in chemistry blanks prepared with MilliQ water onboard the research vessel ($n = 4$) and in the laboratory at ETH Zürich ($n = 10$). On average, a ^{236}U/^{233}U atom ratio of $(2.7 \pm 0.4) \times 10^{-4}$ ($n = 14$) was measured in the blanks, with no significant differences between ship blanks and lab blanks.

3. Results

3.1. ^{129}I and ^{236}U in Depth Profiles

Temperature and salinity data as well as measured ^{129}I, ^{236}U, and ^{238}U concentrations of all samples and the ^{236}U/^{238}U and ^{129}I/^{236}U atom ratios are given in Table S1.

The ^{129}I concentrations measured in the Fram Strait in 2016 ranged between $(2.9 \pm 0.1) \times 10^{7}$ at·kg^{-1} and $(629 \pm 15) \times 10^{7}$ at·kg^{-1}, with a dynamic range of about 200. ^{236}U/^{238}U atom ratios were measured between $(370 \pm 25) \times 10^{-12}$ and $(2,900 \pm 110) \times 10^{-12}$ and ^{236}U concentrations between $(3.1 \pm 0.2) \times 10^{6}$ at·kg^{-1} and $(24.2 \pm 0.8) \times 10^{6}$ at·kg^{-1}, corresponding to a dynamic range of about 8. In general, concentrations of both radionuclides were the highest in surface waters between 0 and 500 m depth and decreased toward greater depths. In contrast to the ^{236}U concentration, the ^{236}U/^{238}U ratio accounts for salinity differences in the samples, as the concentration of natural ^{238}U generally correlates with salinity (Figure S2; Owens et al., 2011; Pates & Muir, 2007).

In the eastern part of the Fram Strait (stations 15, 27, 28, and 37) ^{129}I concentrations ranged from 200–300 $\times 10^{7}$ at·kg^{-1} in the upper 100 m and decreased down to about 10 $\times 10^{7}$ at·kg^{-1} at deep stations (i.e., 28 and 37 with bottom depths below 1,000 and 2,000 m, respectively; Figure 2a, dark blue). In contrast, ^{236}U concentrations (and ^{236}U/^{238}U ratios) were rather homogeneous throughout the upper 500 m of the water column and ranged between 12 and 13 $\times 10^{6}$ at·kg^{-1}. Below 1,000-m depth ^{236}U concentrations decreased down to about 6 $\times 10^{6}$ at·kg^{-1} (Figure 2a, red).

The deepest stations were located in the middle of the Fram Strait at around 0°E, with bottom depths of up to 3,200 m (stations 44, 52, and 103). The ^{129}I profiles all presented a similar trend with concentrations of 300–450 $\times 10^{7}$ at·kg^{-1} at the surface (< 100 m), which gradually decreased down to < 5 $\times 10^{7}$ at·kg^{-1} below 2,000 m depth (Figure 2b, dark blue). Between 100 to 300 m depth, concentrations of ^{129}I were constant at around 200 $\times 10^{7}$ at·kg^{-1}. ^{236}U concentrations were high at the surface (up to 20 $\times 10^{6}$ at·kg^{-1} at station 52) and showed a pronounced local maximum at about 500 m depth (17–20 $\times 10^{6}$ at·kg^{-1}). ^{236}U/^{238}U ratios exhibited a similar behavior with depth. At depths greater than 1,500 m, ^{236}U concentrations fell below 10 $\times 10^{6}$ at·kg^{-1} (Figure 2b, red).

Closer to the Greenland shelf break (stations 56, 101, 280, and 285) seawater samples exhibited the highest concentrations of both radionuclides. For ^{129}I, concentrations increased from about 200 $\times 10^{7}$ at·kg^{-1} at 300-m depth up to 600 $\times 10^{7}$ at·kg^{-1} in surface waters (Figure 2c, dark blue). In the upper 500 m, ^{236}U concentrations ranged from 15 to 25 $\times 10^{6}$ at·kg^{-1}, with highest concentrations between 100 and 300 m depth (Figure 2c, red). This also held for ^{236}U/^{238}U ratios, even though the maximum was less prominent.

At the stations located on the Greenland shelf, bottom depths are only up to 500 m (stations 66, 82, 90, 94, 135, 165, 189, and 241). Some stations (82, 90, 165, and 189) showed decreased ^{129}I concentrations in the surface-most sample, however, in most stations ^{129}I increased toward the surface (Figure 2d, dark blue). ^{236}U concentrations ranged between 15–25 $\times 10^{6}$ at·kg^{-1} throughout the water column (Figure 2d, red). Close to the coast of Greenland, maximum ^{236}U concentrations and ^{236}U/^{238}U ratios were found at about 100 m depth.

Overall, concentrations of both radionuclides were significantly higher in outflowing Arctic waters located in the western part of the Fram Strait, including the Greenland shelf. Differences between the ^{129}I and ^{236}U distribution were observed: whereas ^{129}I concentrations strongly increased toward the surface within the upper 500 m depth, from 200 $\times 10^{7}$ at·kg^{-1} to > 600 $\times 10^{7}$ at·kg^{-1}, ^{236}U concentrations showed a more homogeneous distribution scattering between 10 and 15 $\times 10^{6}$ at·kg^{-1} in the eastern Fram Strait and 15–25 $\times 10^{6}$ at·kg^{-1} in the western Fram Strait. This pattern also held for ^{236}U/^{238}U ratios, which ranged between 1–1.5 $\times 10^{-9}$ and 2–3 $\times 10^{-9}$ in the eastern and western parts, respectively.
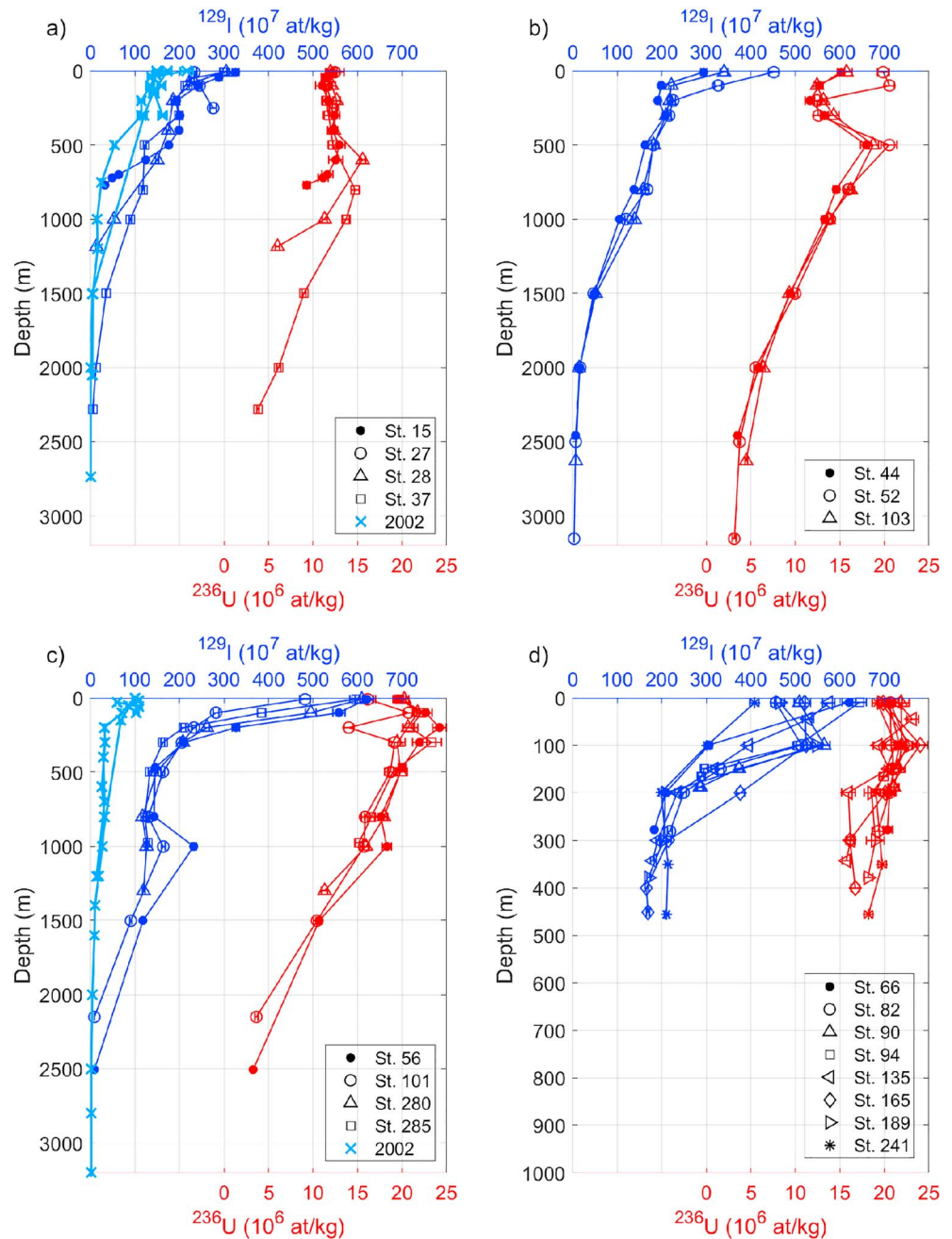
Figure 2. (a–d) Depth profiles with ^{129}I concentration (dark blue, in 10^7 at·kg^{-1}) and ^{236}U concentration (red, in 10^6 at·kg^{-1}) for all stations, grouped by longitude (from east to west). Note the different depth scale for (d). Light blue profiles in (a) and (c) correspond to ^{129}I data from 2002 (Alfimov, Aldahan, & Possnert, 2004).

3.2. Distribution of ^{129}I and ^{236}U in Water Masses

The distribution of ^{129}I and ^{236}U could be associated to the different water masses present in the Fram Strait according to their T-S properties (Figure 3), based on Rudels (2009). The WSC, composed of Atlantic waters, was characterized by the highest potential temperature ($T_{pot} > 2$) and salinity (34.5–35.5). Low densities were found in WSC surface samples and were presumably due to freshwater input from Svalbard. In contrast, the PSW had low potential temperatures of $-2 - 0$ °C and low salinities, ranging between 29.5 and 34.5. Very low salinities indicated a high proportion of meltwater. Surface samples in the middle of the Fram Strait (stations 44, 101, and 103) with salinities < 34.5 and $T_{pot} > 0$ were considered a mixture of
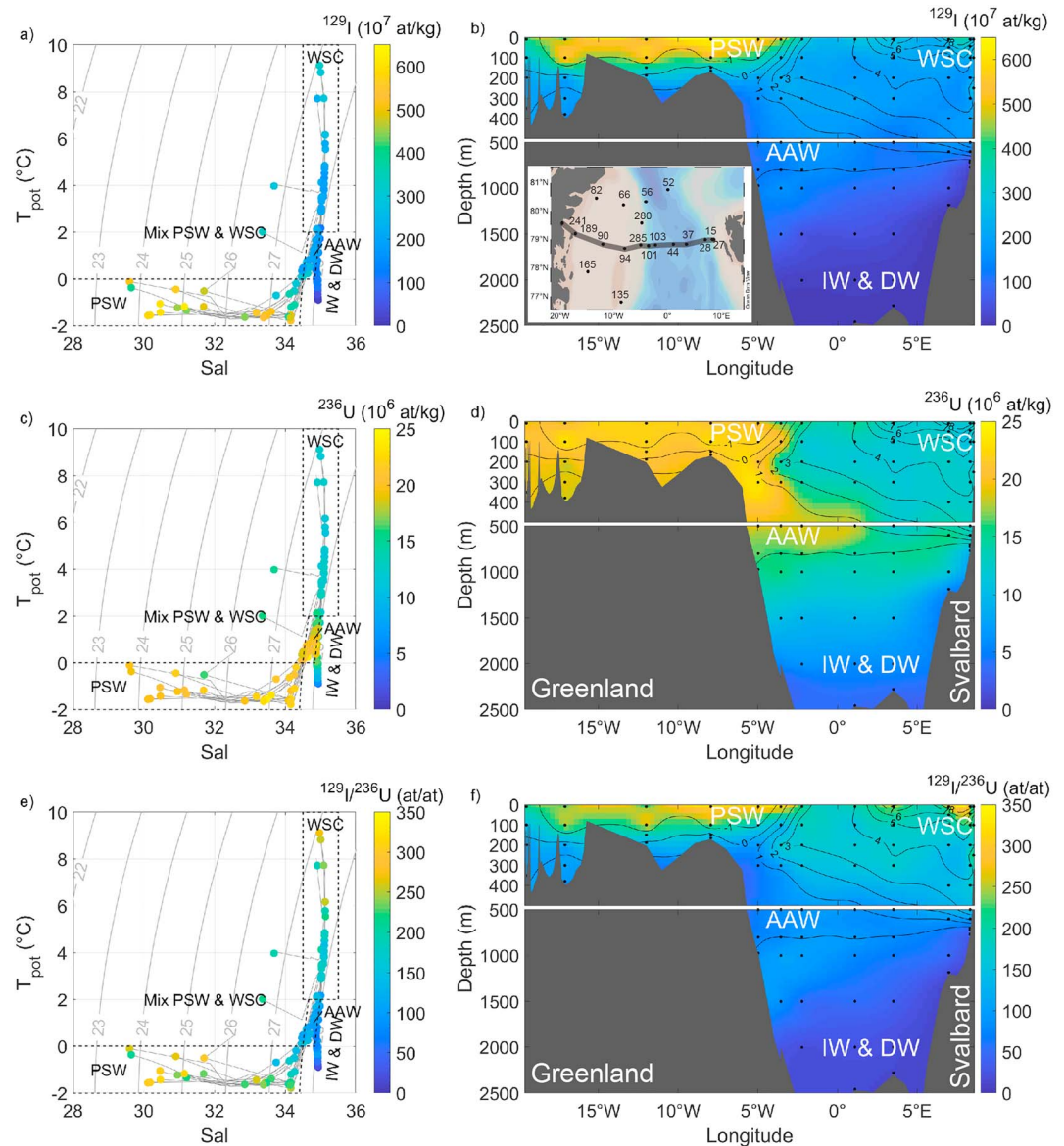
Figure 3. (a) T-S diagram with isopycnals. The colored dots represent [129]I concentration. (b) 79°N transect for [129]I concentrations. (c) Same as (a) but representing [236]U concentration. (d) 79°N transect for [236]U concentrations. (e) Same as (a) but representing [129]I/[236]U atom ratio. (f) 79°N transect for [129]I/[236]U atom ratio. Water masses were defined according to Rudels (2009). WSC, West Spitsbergen Current; PSW, Polar Surface Water; AAW, Arctic Atlantic Waters; IW and DW, Intermediate and Deep Waters. The transect is shown in the inset in (b), black contours in (b), and (d) and (f) depict temperature isolines.

WSC and PSW waters. Below the surface currents, Arctic Atlantic Water (AAW) was the prevailing water mass, covering depths of approximately 300–800 m (Schlichtholz & Houssais, 2002). This water mass corresponds to waters of Atlantic origin that have circulated through the Arctic Ocean, descended from the surface, and have been altered due to various processes, including cooling by atmospheric influence as well as sea ice melt. The AAW was characterized by temperatures between 0 and 2 °C and covered a density range of 27.7–27.97 (Rudels, 2009). Waters below the AAW were distinguished by low potential temperatures and high densities and are here summarized as intermediate and deep waters (IW and DW), originating from different Arctic basins.

The distribution of [129]I and [236]U is coherent with the different water masses described in Rudels (2009). The highest concentrations of [129]I were associated to the PSW, about twice as large as concentrations in the WSC.

^{129}I concentrations decreased rather continuously with depth, from AAW to IW and DW, where lowest concentrations were present (Figure 3a). Regarding the geographical distribution, differences between the eastern and western part of the transect were depicted in the 79°N section (Figure 3b). High ^{129}I concentrations are restricted to surface waters (0-100 m depth) on the Greenland shelf and at the shelf break, in the western part of the Fram Strait.

In the case of ^{236}U, highest concentrations were found in the PSW and the AAW, both higher compared to the WSC (Figure 3c). Again, lowest concentrations were found in deepest waters. As for the ^{129}I, highest ^{236}U concentrations are present in the PSW (Figure 3d). Regarding the distribution with depth, however, ^{236}U was still present in significant amounts at greater depths compared to ^{129}I. High concentrations were found throughout the whole water column on the Greenland shelf and in the AAW at the shelf-break at around 500 to 1,000 m depth, reaching eastward to about 0° E.

Both ^{129}I and ^{236}U profiles showed a dilution of the surface samples in stations close to the Greenland coast (Figure 2d), which decreased radionuclide concentrations by about 10%. Regarding the salinity of the PSW samples, we found a coherent decrease in salinity for those samples, from about 33 in the core of the PSW down to 30 closer to the coast. This suggests the dilution of the surface layer with freshwater that did not carry any tracer signal of ^{129}I or ^{236}U.

Regarding the ^{129}I/^{236}U ratio (Figures 3e and 3f), we see a similar geographical pattern as for the ^{129}I concentrations, suggesting that the concentration of this radionuclide is the main driver for differences in the ratio. The ^{129}I/^{236}U transect will be further explained in the discussion (section 4.2).

4. Discussion

4.1. Time Evolution of ^{129}I and ^{236}U in the Fram Strait

^{129}I and ^{236}U concentrations measured in samples from the WSC were significantly lower compared to the outflowing PSW in the EGC. This finding was not unexpected, as RP releases of ^{129}I and ^{236}U have changed significantly over time and especially the ^{129}I releases increased sharply during the 1990s and rather decreased or stabilized after 1998 (Figure S1a). ^{129}I concentrations have been measured in numerous samples from the Arctic Ocean, collected from the early 1990s until today, and it was found that the increased release of ^{129}I was well reflected in the seawater samples, especially in shallow depths (Alfimov, Aldahan, Possnert, & Winsor, 2004; Smith et al., 2011). Previous studies suggested a transit time of about 2 years from the North Sea to the WSC and about 12–15 years through the Arctic and back to the Fram Strait as PSW (Christl, Casacuberta, Vockenhuber, et al., 2015; Smith et al., 2011). Thus, higher ^{129}I concentrations in the outflowing EGC compared to the inflowing WSC in 2016 are consistent with the decreased ^{129}I releases by RP facilities after 1998. This also holds true for the ^{236}U releases that peaked in the 1980s and had been overall decreasing since 1995 (Figure S1b). Our interpretation is further corroborated when comparing our results (samples in 2016) with the concentrations of ^{129}I in the Fram Strait obtained in 2002 (Alfimov, Aldahan, & Possnert, 2004; Figures 2a and 2c, light blue profiles). In the 14 years elapsed between the two studies, ^{129}I concentrations in surface waters of the WSC (entering the Arctic Ocean) increased about 1.5 times (Figure 2a) while the PSW (outflowing the Arctic Ocean) show a six-fold increase of ^{129}I concentrations (Figure 2c). The time evolution of ^{129}I in both the WSC and the PSW therefore reflects the dynamics of the ^{129}I input function from RP (with its sharp increase in the 1990s) and the different transit times of waters from the North Sea to either the inflow or the outflow of Atlantic waters to and from the Arctic Ocean. The use of the input function to calculate transit times of water masses is discussed in section 4.3.

4.2. Constraining Sources of ^{129}I and ^{236}U in the Fram Strait

Up to date, nearly all studies using RP-derived artificial radionuclides as tracers of circulation in the Arctic and North Atlantic Ocean considered SF and LH as a combined single point-like source. In other words, the releases from SF and LH that enter the North Sea would first completely mix before continuing northward with the NCC forming a single RP input function for the Arctic Ocean (e.g., Christl, Casacuberta, Vockenhuber, et al., 2015; Smith et al., 2005, 2011).

Yet a recent study (Casacuberta et al., 2018) found that the ^{129}I and ^{236}U signals from LH and SF do not completely mix in the North Sea, suggesting three different input functions for Atlantic waters entering the
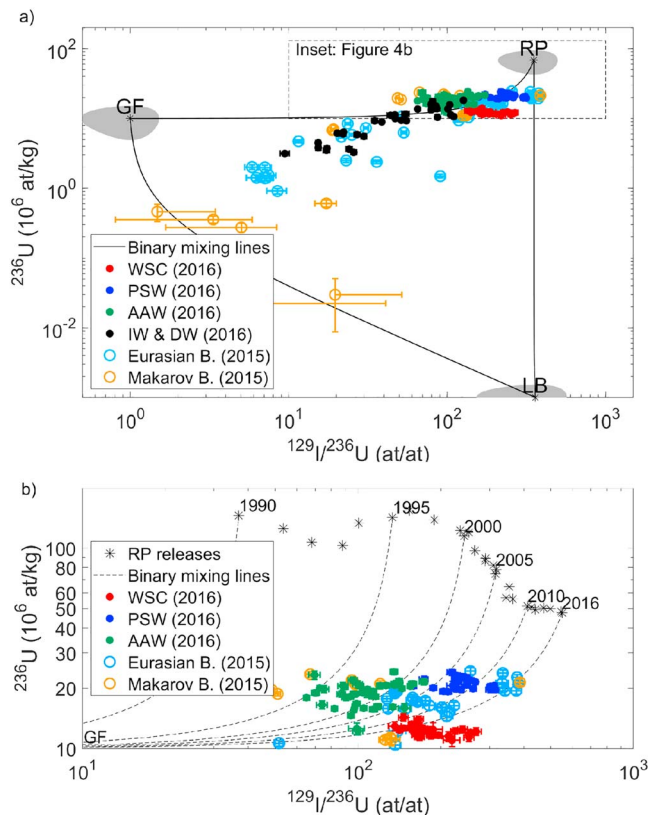
Figure 4. (a) Dual-tracer plot for steady-state end-member sand using a single input function for the reprocessing plants (RPs). The RP end-member corresponds to an average value of the years 2000–2016, with 68×10^6 at·kg^{-1} ^{236}U and a ^{129}I/^{236}U ratio of 350. LB, lithogenic background; GF, global fallout. Note that in reality, a direct mixture between LB and RP is not possible for the Fram Strait study area. The gray areas are uncertainty estimates for the end-members based on Casacuberta et al. (2016). The inset in (a) is shown in (b). Data from 2015 are taken from Casacuberta et al. (2018). Fram Strait samples from this study are sorted by water masses according to T-S properties. Three samples that were identified as a mixture of PSW and WSC are not shown. (b) Time-dependent dual-tracer plot for dilution between RP and GF only. RP releases are shown for individual years from 1990–2016 (Christl, Casacuberta, Vockenhuber, et al., 2015); the GF value is kept constant as in (a). Note that both plots are in log-log scale; hence, mixing lines are curved.

Arctic Ocean (two branches entering via Barents Sea, green and purple in Figure 1a and one via Fram Strait, orange in Figure 1a). The high ^{129}I/^{236}U ratio released from LH largely remains within the NCC, which enters the Barents Sea very close to the Norwegian coast. This coastal current mainly stays at the surface and close to the shelf before it enters the Eurasian Basin via the Laptev Sea (green arrow in Figure 1a). In Casacuberta et al. (2018) this branch was labeled Arctic Shelf Break Branch (Aksenov et al., 2011). However, since our definition of this branch does not fully concur with the definition of Arctic Shelf Break Branch by Aksenov et al. (2011) we hereafter refer to this branch as NCC Branch Water, NCC$_{BW}$. The NCC$_{BW}$ is, among others, a source of low-salinity shelf waters in the Kara and Laptev Sea (Rudels et al., 2004). This branch therefore presents a pathway of ^{129}I and ^{236}U to the Arctic Ocean that can in particular be associated to surface water concentrations in the Nansen, Amundsen, and potentially also the Makarov Basin. These waters ultimately evolve into the surface waters of the EGC present in the Fram Strait. The other two Atlantic branches entering the Arctic Ocean (FSBW and BSBW) are known to circulate through the Arctic Ocean at depths of 300–800 m (Aksenov et al., 2011; Rudels et al., 2015). Therefore, the tracer input functions for FSBW and BSBW are assumed to be representative for the AAW in the Fram Strait.

In sections 4.2.1 and 4.2.2 we discuss the ^{129}I and ^{236}U data obtained in the Fram Strait considering the following three approaches: (i) a steady-state, three end-member mixing model; (ii) one single input function coming from a combined RP signal; and (iii) three different input functions for the FSBW, BSBW, and NCC$_{BW}$.

4.2.1. Steady-State Approach and Single Input Function From RP

In order to distinguish between the different sources of ^{129}I and ^{236}U, that is, lithogenic background (LB), GF, and RPs, the dual-tracer approach of using the ^{236}U/^{238}U ratio together with the ^{129}I/^{236}U atom ratio has been successfully applied in previous studies (Casacuberta et al., 2016; Castrillejo et al., 2018). For convenience, here we use the ^{236}U concentrations instead of the ^{236}U/^{238}U, as conclusions would be similar.

^{236}U concentrations and ^{129}I/^{236}U ratios for LB and GF have been defined in Casacuberta et al. (2016). For a steady-state approach we averaged over the time-dependent RP releases from 2000 to 2012 (Christl, Casacuberta, Vockenhuber, et al., 2015). In the dual-tracer plot, these three sources are plotted as end-members, together with binary mixing lines (Figure 4a). The GF end-member is characterized by surface ^{236}U concentrations of about 10×10^6 at·kg^{-1} and a ^{129}I/^{236}U ratio of 1. Averaged RP releases since 2000 resulted in about seven times higher ^{236}U concentrations compared to GF and a high ^{129}I/^{236}U ratio of 330. The natural, LB is distinguished by extremely low ^{236}U concentrations of 0.001×10^6 at·kg^{-1} and an estimated ^{129}I/^{236}U ratio of > 300. A direct dilution between RP and LB is not considered as the RP signal is introduced into the surface and all intermediate-depth waters (in the northern hemisphere) are tagged with GF. A pure LB signal can only be found in deep and old waters that cannot have been in direct contact with RP-tagged waters before having seen the GF signal. Therefore, waters tagged with RP will first dilute with waters having GF input and subsequently mix with the LB end-member.

Samples presented in this work are plotted by water masses according to the definition in section 3.2 (see Table S1). For comparison, a subset of samples from the Arctic Ocean (Eurasian Basin and Makarov Basin) collected in 2015 is also shown (Casacuberta et al., 2018; Figure 4a). Most of the Fram Strait samples plot within the domain defined by the three steady-state end-members. Surface samples (PSW and WSC) as well as the AAW plot close to the RP end-member and partly scatter around the GF-RP mixing line. As

expected, most IW and DW have less RP influence due to their long isolation times, plotting closer to the GF-LB mixing line.

In this dual-tracer plot, we find two features that are not consistent with the simple steady-state mixing model (approach (i)): first, some AAW samples plot above the GF-RP mixing line due to very high ^{236}U concentrations, therefore being out of the domain defined by the three end-members; second, PSW samples show a higher proportion of the RP end-member compared to the inflowing WSC. Since the PSW are outflowing waters from the Arctic Ocean, one would have expected it to plot closer to the GF end-member than the WSC due to greater dilution of the RP signal along the flow.

To investigate this in more detail, we consider that the RP end-member is in fact not in steady state but has been changing significantly over time (Figure S1; approach (ii)). The RP releases are therefore plotted separately for the years 1990–2012 (Christl, Casacuberta, Vockenhuber, et al., 2015), together with individual GF dilution lines for several years (Figure 4b). We indeed observe that the AAW samples are largely influenced by RP releases prior to 2002, which are characterized by high ^{236}U concentrations and low ^{129}I/^{236}U ratios. This therefore solves the first inconsistent feature observed in the dual-tracer plot but not the fact that the PSW are less diluted by GF (plot closer to the RP end-member) than the WSC. Concerning this last feature, two hypotheses were taken into account: (i) the presence of an additional source of ^{129}I (and ^{236}U) in the Arctic Ocean leading to a high ^{129}I/^{236}U ratio and (ii) different ^{129}I and ^{236}U input functions to the WSC and the PSW, respectively, due to different mixing proportions of the La Hague and Sellafield streams in the North Sea (Casacuberta et al., 2018).

Regarding hypothesis (i) the addition of ^{129}I (and ^{236}U) to the PSW implies a source associated to low density waters, for example, riverine input or sea ice melt. Previous studies have been conducted on Russian rivers as potential sources of anthropogenic radionuclides in the Arctic Ocean (Beasley et al., 1998; Casacuberta et al., 2016; Cooper et al., 1999; Moran et al., 1995). Maximum concentrations of ^{129}I measured in the Ob river in 1994 were about 280×10^7 at·l^{-1} (Moran et al., 1995), which is significantly lower than ^{129}I concentrations in the EGC samples 2016. There is no data available from the Ob river from different years, however, so the impact on ^{129}I (and ^{236}U) in the Arctic Ocean remains unclear. The Lena river was excluded as a source of both ^{129}I and ^{236}U based on samples collected in the mouth of the river in 2014 (6–11 $\times 10^7$ at·kg^{-1} ^{129}I and 3–4 $\times 10^6$ at·kg^{-1} ^{236}U; Casacuberta et al., 2016). In a recent study, ^{129}I and ^{236}U concentrations in sea ice cores collected in the Arctic Ocean in 2015 were presented (Casacuberta et al., 2018). Maximum concentrations of 105×10^7 at·l^{-1} ^{129}I and 1.9×10^6 at·l^{-1} ^{236}U in the ice cores do not support sea ice melt as a source of ^{129}I and ^{236}U to the surface waters.

4.2.2. Using Three Different Atlantic Branches to Explain ^{129}I and ^{236}U in the Fram Strait

In approach (iii) we consider three different Atlantic branches (i.e., FSBW, BSBW, and NCC$_{BW}$) entering the Arctic Ocean with three different input functions for both ^{129}I and ^{236}U (Casacuberta et al., 2018). Briefly, for the construction of the new, separate input functions, the existing input functions for GF, SF, and LH branch waters (Christl, Casacuberta, Vockenhuber, et al., 2015) were considered as separate, individual sources. The relative contributions of SF, LH, and GF to the three branches (FSBW, BSBW, and NCC$_{BW}$) were assumed to be constant over time and determined using a three-end-member mass balance based on measurements of ^{129}I and ^{236}U concentrations in the WSC and across the Barents Sea (Casacuberta et al., 2018). The NCC$_{BW}$ was defined at the northern Norwegian coast (around 72°N), the BSBW at the entrance to the Barents Sea around 72–74°N, and the FSBW at around 79°N in the WSC west of Svalbard.

The newly defined input functions for FSBW, BSBW, and NCC$_{BW}$ indicate maximum ^{129}I/^{236}U ratios of about 400 and 220 for the BSBW and the FSBW, respectively (Figure S3c). The NCC$_{BW}$, in contrast, shows higher ^{129}I/^{236}U ratios of more than 700, which is mainly due to the fact that it carries a significant fraction of the LH RP that has released more ^{129}I compared to SF. Already in a previous study on seawater samples taken close to the coast of Norway (in the Lofoten Basin and at the entrance of the Barents Sea), extremely high ^{129}I concentrations were observed (Gascard et al., 2004).

Following approach (iii) with three separate input functions, ^{236}U concentrations and ^{129}I/^{236}U ratios of each branch spanning from 1990 to 2015 are plotted together with the respective dilution lines with the GF end-member (Figure 5). Results of this study, together with data from the Arctic Ocean from
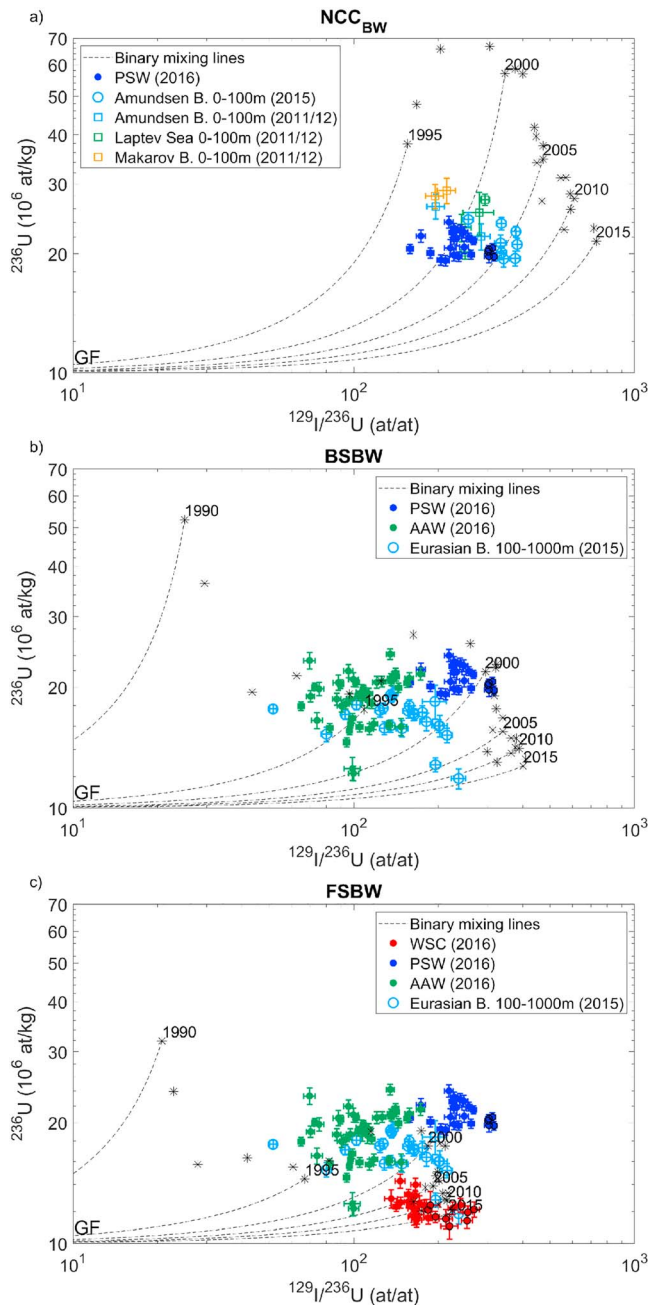
Figure 5. Dual-tracer plots (dilution with global fallout only) for the three new input functions of ^{129}I and ^{236}U into the Arctic Ocean (from Casacuberta et al., 2018); (a) Norwegian Coastal Current Branch Water (NCC$_{BW}$), (b) Barents Sea Branch Water (BSBW), and (c) Fram Strait Branch Water (FSBW). Data from 2011/2012 are taken from Casacuberta et al. (2016); data from 2015 are taken from Casacuberta et al. (2018).

2011/2012 (Casacuberta et al., 2016) and 2015 (Casacuberta et al., 2018), are superimposed on the binary mixing model.

As mentioned above, we expect the PSW to be an evolution of the NCC$_{BW}$, as the BSBW and the FSBW circulate the Arctic Ocean in greater depths and evolve into the AAW. The PSW samples are therefore compared to the NCC$_{BW}$ input function (Figure 5a). As expected, they fall on dilution lines of the NCC$_{BW}$ end-member with GF. A subset of PSW samples located at the Greenland shelf break (dark blue circles with black outline; Figure 5a) has higher $^{129}I/^{236}U$ ratios. These samples probably represent the core of the PSW in the EGC that is not affected by recirculation on the shelf and are therefore less diluted with older waters having a lower $^{129}I/^{236}U$ ratio. For completeness, the PSW samples are also compared to the BSBW and the FSBW input functions (Figures 5b and 5c, respectively). Here the data plots extremely close to the BSBW end-member meaning that no dilution would have occurred in these waters from the Barents Sea to the PSW, which is not a realistic scenario. Regarding the FSBW input function, the PSW samples do always plot beyond the domain defined by the binary mixing lines, again being a nonrealistic scenario. Surface data (0–100 m) from the Amundsen Basin (2011/2012 and 2015), the Laptev Sea, and the Makarov Basin (2011/2012) plot slightly closer to the NCC$_{BW}$ end-member input function compared to the PSW samples. Overall, this supports the hypothesis of the NCC$_{BW}$ bringing ^{129}I and ^{236}U to the surface of the Arctic Ocean via the Laptev Sea and implies that the PSW is an evolution of surface waters in the Amundsen and Makarov basins. The fact that the Laptev Sea and Makarov Basin samples plot closer to the PSW samples than the NCC$_{BW}$ end-member furthermore suggests that the dilution mostly takes place on the Arctic shelf.

The BSBW input function is expected to bring ^{129}I and ^{236}U to the mid-depth Atlantic layer in the Arctic Ocean. Therefore, Eurasian Basin samples from 2015 (100 to 1,000 m depth) and AAW samples from 2016 can be hydrographically assigned to the BSBW. Results show that the AAW samples plot close to the BSBW input function around year 1995 but with very little dilution of the RP signal during circulation through the Arctic Ocean (Figure 5b). This implies that little dilution takes place in the deep basins. Another possible explanation could rely on the interaction of BSBW with the NCC$_{BW}$ along the flow in the Barents Sea, which would result in an increase of both ^{129}I and ^{236}U in the BSBW. Middepth samples (Eurasian Basin and AAW) could in principle also be an evolution of the FSBW (Figure 5c). Regarding the FSBW input function, however, they largely fall out of the domain due to high ^{236}U concentrations. This either suggests that also the FSBW interacts with the coastal current (i.e., NCC$_{BW}$) or that the AAW in 2016 mainly evolves from BSBW with no influence of the FSBW observed in our study area. It could also be possible that the assumptions for defining the new input functions with constant proportions of SF, LH, and GF are not constant in time. Samples from the WSC core (black outline, Figure 5c) have been used to define the

FSBW input function in Casacuberta et al. (2018) and consequently match GF dilution lines from recent years, together with the rest of the WSC.

Finally, comparing the PSW samples in the NCC$_{BW}$ (Figure 5a) and the WSC samples in the FSBW (Figure 5c), we clearly see a stronger dilution of the PSW, which is expected for the evolution of NCC$_{BW}$ circulating through the Arctic Ocean. Reconsidering the 79°N transect of ^{129}I and ^{236}U (Figure 3), the high ^{129}I concentrations only within the upper 100 m of the EGC can clearly be attributed to the NCC$_{BW}$, which
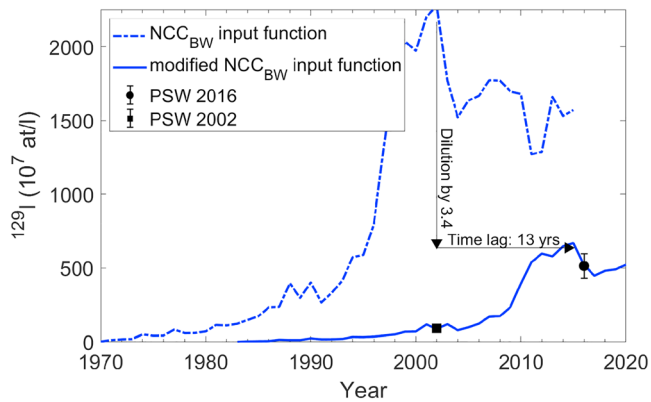
Figure 6. Average Polar Surface Water (PSW) ^{129}I concentrations measured in 2002 (Alfimov, Aldahan, & Possnert, 2004) and 2016, together with NCC$_{BW}$ input function for ^{129}I (Casacuberta et al., 2018). A dilution factor of 3.4 ± 0.6 and a time lag of 13 ± 3 years was applied to the input function to match the measured ^{129}I concentrations.

remains in the surface. Low concentrations of ^{129}I found in the AAW support the small proportion of LH as the main source of ^{129}I in the FSBW and BSBW, compared to the NCC$_{BW}$ (Casacuberta et al., 2018). A higher proportion of SF and GF in the FSBW and BSBW, bringing mainly the ^{236}U signal, is in line with higher ^{236}U concentrations measured in the AAW.

In summary, three separate input functions for ^{129}I and ^{236}U in the NCC$_{BW}$, FSBW, and BSBW are consistent with the observed concentrations of both radionuclides measured in the Fram Strait in 2016 and in the Eurasian basin in 2015. This supports the assumption that one single input function for ^{129}I and ^{236}U is not sufficient to describe the distribution and the temporal behavior of those radionuclides in the Arctic Ocean. Although additional radionuclide input through the Ob, Yenisei, or Lena rivers cannot be excluded due to a lack of data, it is not required to quantitatively explain the observed ^{129}I and ^{236}U concentrations as well as ^{129}I/^{236}U ratios measured in the PSW. The dual-tracer approach using the three individual input functions for NCC$_{BW}$, BSBW, and FSBW serves to constrain the origin of different waters in the Arctic Ocean and is applied for an estimation of transit times in the following.

4.3. Estimation of Transit Times of Atlantic Waters in the Fram Strait

Transit times of Atlantic waters from the entrance of the Arctic Ocean (where input functions were defined) to the Fram Strait can be estimated using the binary mixing lines of the single RP, NCC$_{BW}$, or BSBW end-member with GF. To this purpose, we take the difference between sampling year and the binary mixing lines that correspond to the respective sample subset associated with the input function in the dual-tracer plots.

Using the NCC$_{BW}$ input function, PSW samples point to transit times of 12–19 years (Figure 5a) from the entrance of the Barents Sea (northern Norwegian coast) to the surface EGC at 79°N (corresponding to flow of the NCC$_{BW}$; Figure 1a, green). The PSW samples at the shelfbreak (dark blue circles with black outline, Figure 5a) show slightly shorter transit times. Amundsen Basin samples from 2011/2012 plot on dilution lines from 1999 to 2002, corresponding to transit times of 9–13 years. As expected, the samples collected at the Laptev Sea in 2011/2012 show a shorter transit time (9–10 years) compared to samples taken at the Makarov Basin (13–14 years) in the same year. Finally, the samples collected in the Amundsen Basin in 2015 mainly plot on dilution lines between 2004 and 2007 (8–11 years transit time), hence about 5 years later compared to the 2011/2012 samples taken at a similar location.

The AAW, following the dilution of the BSBW input function, would account for a transit time of about 16–23 years from the entrance to the Barents Sea south of Svalbard to the middepth Atlantic layer (AAW) of the Fram Strait (Figure 5b). This is in line with previous studies, suggesting that the BSBW partly also circulates through the Canadian Basin, whereas the surface flow of the NCC$_{BW}$ is probably confined to the Eurasian Basin (Rudels et al., 2004).

Another way of estimating transit times to the Fram Strait is based on a time series of data. For this, we use the averaged ^{129}I concentrations measured in the upper 100 m of the EGC in 2002 (Alfimov, Aldahan, & Possnert, 2004) and 2016 (this study; Figure 6) and the NCC$_{BW}$ input function. To match the data, a time lag of about 13 ± 3 years together with a dilution factor of 3.4 ± 0.6 is applied. This fits well to 12–16 years resulting from the dual-tracer plot using the NCC$_{BW}$ input function and is in general agreement with previous studies that suggest Atlantic water transit times of about 7–11 years from 60°N to the surface of the Amundsen Basin (Smith et al., 2011).

However, in order to better constrain transit times of waters in the EGC, a well-resolved time series of data would be needed. To take into account interannual mixing within one branch, the concept of transit-time distributions has been applied, also using ^{129}I together with ^{137}Cs and CFCs (Smith et al., 2011). With the newly defined input functions of ^{129}I and ^{236}U to the Arctic Ocean, this approach can be extended and transferred to the combination of ^{129}I and ^{236}U in future studies.

5. Conclusions

This study presents results of ^{129}I and ^{236}U measurements in seawater samples collected during the R/V Polarstern expedition PS100 in the Fram Strait in 2016. Overall, higher concentrations of both radionuclides were found in the outflowing surface waters from the Arctic Ocean, the PSW as part of the EGC. These were about twice as high as those entering the Arctic Ocean through the WSC. Previous studies assumed a single, combined input function for ^{129}I and ^{236}U releases from the two European RPs and GF that enters the Arctic Ocean via the FSBW and the BSBW. The high concentrations of ^{129}I and ^{236}U measured in the PSW in 2016, however, confirm recent studies indicating the substantial role of modified NCC waters, here referred to as NCC Branch Water (NCC$_{BW}$). This surface current carries a significantly larger proportion of ^{129}I and ^{236}U from RP compared to the FSBW and the BSBW, which should in addition be considered as two branches carrying different input functions. Therefore, one can use the ^{129}I/^{236}U ratio to distinguish between the three Atlantic branches in the Arctic Ocean and in the Fram Strait.

In this study, we use the three different input functions of ^{129}I/^{236}U for the FSBW, BSBW, and NCC$_{BW}$ to understand the distribution of ^{129}I and ^{236}U in the Fram Strait and to apply first estimates of water mass transit times. In the Fram Strait, outflowing Arctic Atlantic waters, the middepth Atlantic layer, can be associated to the BSBW input function rather than the FSBW. The PSW, however, seems to contain a large proportion of the NCC, characterized by high ^{129}I/^{236}U ratios. Finally, transit times for the NCC$_{BW}$ and the BSBW to the Fram Strait have been estimated to be about 12–19 years and 16–23 years, respectively, supporting previous results. This study therefore highlights that the combination of the long-lived radionuclides ^{129}I and ^{236}U is a valuable tool for the determination of transit times of Atlantic waters in the North Atlantic and Arctic Ocean.

References

Aksenov, Y., Ivanov, V. V., Nurser, A. J., Bacon, S., Polyakov, I. V., Coward, A. C., et al. (2011). The arctic circumpolar boundary current. *Journal of Geophysical Research*, *116*, C09017. https://doi.org/10.1029/2010JC006637

Aldahan, A., Alfimov, V., & Possnert, G. (2007). ^{129}I anthropogenic budget: Major sources and sinks. *Applied Geochemistry*, *22*(3), 606–618. https://doi.org/10.1016/j.apgeochem.2006.12.006

Alfimov, V., Aldahan, A., & Possnert, G. (2004). Tracing water masses with ^{129}I in the western Nordic Seas in early spring 2002. *Geophysical Research Letters*, *31*, L19305. https://doi.org/10.1029/2004GL020863

Alfimov, V., Aldahan, A., & Possnert, G. (2013). Water masses and ^{129}I distribution in the Nordic Seas. *Nuclear Instruments and Methods in Physics Research Section B Beam Interactions with Materials and Atoms*, *294*, 542–546. https://doi.org/10.1016/j.nimb.2012.07.042

Alfimov, V., Aldahan, A., Possnert, G., Kekli, A., & Meili, M. (2004). Concentrations of ^{129}I along a transect from the North Atlantic to the Baltic Sea. *Nuclear Instruments and Methods in Physics Research Section B Beam Interactions with Materials and Atoms*, *223-224*, 446–450. https://doi.org/10.1016/j.nimb.2004.04.084

Alfimov, V., Aldahan, A., Possnert, G., & Winsor, P. (2004). Anthropogenic iodine-129 in seawater along a transect from the Norwegian Coastal Current to the North Pole. *Marine Pollution Bulletin*, *49*(11-12), 1097–1104. https://doi.org/10.1016/j.marpolbul.2004.08.019

Beasley, T., Cooper, L. W., Grebmeier, J. M., Aagaard, K., Kelley, J. M., & Kilius, L. R. (1998). 237Np/^{129}I atom ratios in the Arctic Ocean: Has 237Np from Western European and Russian fuel reprocessing facilities entered the Arctic Ocean? *Journal of Environmental Radioactivity*, *39*(3), 255–277. https://doi.org/10.1016/S0265-931X(97)00059-3

Beszczynska-Moller, A., Fahrbach, E., Schauer, U., & Hansen, E. (2012). Variability in Atlantic water temperature and transport at the entrance to the Arctic Ocean, 1997-2010. *ICES Journal of Marine Science*, *69*(5), 852–863. https://doi.org/10.1093/icesjms/fss056

Beszczynska-Möller, A., Woodgate, R., Lee, C., Melling, H., & Karcher, M. (2011). A synthesis of exchanges through the main oceanic gateways to the Arctic Ocean. *Oceanography*, *24*(3), 82–99. https://doi.org/10.5670/oceanog.2011.59

Budéus, G., Schneider, W., & Kattner, G. (1997). Distribution and exchange of water masses in the Northeast Water Polynya (Greenland Sea). *Journal of Marine Systems*, *10*(1-4), 123–138. https://doi.org/10.1016/S0924-7963(96)00074-7

Buraglio, N., Aldahan, A., & Possnert, G. (1999). Distribution and inventory of ^{129}I in the central Arctic Ocean. *Geophysical Research Letters*, *26*(8), 1011–1014. https://doi.org/10.1029/1999GL900178

Carmack, E., & Aagaard, K. (1973). On the deep water of the Greenland Sea. *Deep Sea Research and Oceanographic Abstracts*, *20*(8), 687–715. https://doi.org/10.1016/0011-7471(73)90086-7

Casacuberta, N., Christl, M., Lachner, J., Van-der-Loeff, M. R., Masqué, P., & Synal, H. A. (2014). A first transect of ^{236}U in the North Atlantic Ocean. *Geochimica et Cosmochimica Acta*, *133*, 34–46. https://doi.org/10.1016/j.gca.2014.02.012

Casacuberta, N., Christl, M., Vockenhuber, C., Wefing, A.-M., Wacker, L., Masqué, P., et al. (2018). Tracing the three Atlantic branches entering the Arctic Ocean with ^{129}I and ^{236}U. *Journal of Geophysical Research: Oceans*, *123*, 6909–6921. https://doi.org/10.1029/2018JC014168

Casacuberta, N., Masqué, P., Henderson, G., Rutgers van der Loeff, M., Bauch, D., Vockenhuber, C., et al. (2016). First ^{236}U data from the Arctic Ocean and use of ^{236}U/^{238}U and ^{129}I/^{236}U as a new dual tracer. *Earth and Planetary Science Letters*, *440*, 127–134. https://doi.org/10.1016/j.epsl.2016.02.020

Castrillejo, M., Casacuberta, N., Christl, M., Garcia-Orellana, J., Vockenhuber, C., Synal, H. A., & Masqué, P. (2017). Anthropogenic ^{236}U and ^{129}I in the Mediterranean Sea: First comprehensive distribution and constrain of their sources. *Science of the Total Environment*, *593-594*, 745–759. https://doi.org/10.1016/j.scitotenv.2017.03.201

Castrillejo, M., Casacuberta, N., Christl, M., Vockenhuber, C., Synal, H. A., García-Ibáñez, M. I., et al. (2018). Tracing water masses with ^{129}I and ^{236}U in the subpolar North Atlantic along the GEOTRACES GA01 section. *Biogeosciences Discussions*, 1–28. https://doi.org/10.5194/bg-2018-228

Christl, M., Casacuberta, N., Lachner, J., Herrmann, J., & Synal, H. A. (2017). Anthropogenic ^{236}U in the North Sea—A closer look into a source region. *Environmental Science & Technology*, *51*(21), 12,146–12,153. https://doi.org/10.1021/acs.est.7b03168

Christl, M., Casacuberta, N., Lachner, J., Maxeiner, S., Vockenhuber, C., Synal, H. A., et al. (2015). Status of ^{236}U analyses at ETH Zurich and the distribution of ^{236}U and ^{129}I in the North Sea in 2009. *Nuclear Instruments and Methods in Physics Research Section B: Beam Interactions with Materials and Atoms*, *361*, 510–516. https://doi.org/10.1016/j.nimb.2015.01.005

Christl, M., Casacuberta, N., Vockenhuber, C., Elsässer, C., Bailly du Bois, P., Herrmann, J., & Synal, H. A. (2015). Reconstruction of the ^{236}U input function for the Northeast Atlantic Ocean: Implications for ^{129}I/^{236}U and ^{236}U/^{238}U-based tracer ages. *Journal of Geophysical Research: Oceans*, *120*, 7282–7299. https://doi.org/10.1002/2015JC011116

Christl, M., Lachner, J., Vockenhuber, C., Goroncy, I., Herrmann, J., & Synal, H. A. (2013). First data of Uranium-236 in the North Sea. *Nuclear Instruments and Methods in Physics Research Section B: Beam Interactions with Materials and Atoms*, *294*, 530–536. https://doi.org/10.1016/j.nimb.2012.07.043

Christl, M., Lachner, J., Vockenhuber, C., Lechtenfeld, O., Stimac, I., Van-der-Loeff, M. R., & Synal, H. A. (2012). A depth profile of uranium-236 in the Atlantic Ocean. *Geochimica et Cosmochimica Acta*, *77*, 98–107. https://doi.org/10.1016/j.gca.2011.11.009

Christl, M., Vockenhuber, C., Kubik, P. W., Wacker, L., Lachner, J., Alfimov, V., & Synal, H. A. (2013). The ETH Zurich AMS facilities: Performance parameters and reference materials. *Nuclear Instruments and Methods in Physics Research Section B: Beam Interactions with Materials and Atoms*, *294*, 29–38. https://doi.org/10.1016/j.nimb.2012.03.004

Cooper, L. W., Beasley, T., Aagaard, K., Kelley, J. M., Larsen, I. L., & Grebmeier, J. M. (1999). Arctic Ocean: Indications of Russian river influence. *Journal of Marine Research*, *57*(5), 715–738. https://doi.org/10.1357/002224099321560546

Dodd, P. A., Heywood, K. J., Meredith, M. P., Naveira-Garabato, A. C., Marca, A. D., & Falkner, K. K. (2009). Sources and fate of freshwater exported in the East Greenland Current. *Geophysical Research Letters*, *36*, L19608. https://doi.org/10.1029/2009GL039663

Dodd, P. A., Rabe, B., Hansen, E., Falck, E., MacKensen, A., Rohling, E., et al. (2012). The freshwater composition of the Fram Strait outflow derived from a decade of tracer measurements. *Journal of Geophysical Research*, *117*, C11005. https://doi.org/10.1029/2012JC008011

Edmonds, H. N., Smith, J. N., Livingston, H. D., Kilius, L. R., & Edmond, J. M. (1998). ^{129}I in archived seawater samples. *Deep-sea Research. Part I, Oceanographic Research Papers*, *45*(7), 1111–1125. https://doi.org/10.1016/S0967-0637(98)00007-7

Edmonds, H. N., Zhou, Z. Q., Raisbeck, G. M., Yiou, F., Kilius, L., & Edmond, J. M. (2001). Distribution and behavior of anthropogenic ^{129}I in water masses ventilating the North Atlantic Ocean. *Journal of Geophysical Research*, *106*(C4), 6881–6894. https://doi.org/10.1029/1999JC000282

Gascard, J.-C., Raisbeck, G., Sequeira, S., Yiou, F., & Mork, K. A. (2004). The Norwegian Atlantic Current in the Lofoten basin inferred from hydrological and tracer data (^{129}I) and its interaction with the Norwegian Coastal Current. *Geophysical Research Letters*, *31*, L01308. https://doi.org/10.1029/2003GL018303

Hattermann, T., Isachsen, P. E., Von Appen, W. J., Albretsen, J., & Sundfjord, A. (2016). Eddy-driven recirculation of Atlantic Water in Fram Strait. *Geophysical Research Letters*, *43*, 3406–3414. https://doi.org/10.1002/2016GL068323

Hou, X. (2004). Application of ^{129}I as an environmental tracer. *Journal of Radioanalytical and Nuclear Chemistry*, *262*(1), 67–75. https://doi.org/10.1023/B:JRNC.0000040855.91732.9f

Kanzow, T. (2017). The Expedition PS100 of the Research Vessel POLARSTERN to the Fram Strait in 2016. https://doi.org/10.2312/BzPM_0705_2017

Karcher, M., Smith, J. N., Kauker, F., Gerdes, R., & Smethie, W. M. (2012). Recent changes in Arctic Ocean circulation revealed by iodine-129 observations and modeling. *Journal of Geophysical Research*, *117*, C08007. https://doi.org/10.1029/2011JC007513

Kershaw, P., & Baxter, A. (1995). The transfer of reprocessing wastes from north-west Europe to the Arctic. *Deep-sea Research. Part II*, *42*(6), 1413–1448. https://doi.org/10.1016/0967-0645(95)00048-8

Kilius, L. R., Smith, J. N., & Ellis, K. M. (1995). The measurement of I-129 in the Canadian Arctic Basin and other Arctic waters. In P. Strand & A. Cooke (Ed.), *Environ. Radioact. Arctic* (Vol. 2, pp. 117–120). Østerås: Norwegian Radiation Protection Authority.

Killworth, P. D. (1983). Deep convection in the world ocean. *Reviews of Geophysics and Space Physics*, *21*(1), 1–26. https://doi.org/10.1029/RG021i001p00001

Michel, R., Daraoui, A., Gorny, M., Jakob, D., Sachse, R., Tosch, L., et al. (2012). Iodine-129 and iodine-127 in European seawaters and in precipitation from northern Germany. *Science of the Total Environment*, *419*, 151–169. https://doi.org/10.1016/j.scitotenv.2012.01.009

Moran, S. B., Cochran, J. K., Fisher, N. S., & Kilius, L. R. (1995). 129I in the Ob River. In P. Strand & A. Cooke (Eds.), *Environ. Radioact. Arctic* (pp. 75–78). Østerås: Norwegian Radiation Protection Authority.

Orre, S., Smith, J. N., Alfimov, V., & Bentsen, M. (2010). Simulating transport of ^{129}I and idealized tracers in the northern North Atlantic Ocean. *Environmental Fluid Mechanics*, *10*(1-2), 213–233. https://doi.org/10.1007/s10652-009-9138-3

Owens, S. A., Buesseler, K. O., & Sims, K. W. W. (2011). Re-evaluating the ^{238}U-salinity relationship in seawater: Implications for the ^{238}U-^{234}Th disequilibrium method. *Marine Chemistry*, *127*(1-4), 31–39. https://doi.org/10.1016/j.marchem.2011.07.005

Pates, J. M., & Muir, G. K. P. (2007). U-salinity relationships in the Mediterranean: Implications for ^{234}Th:^{238}U particle flux studies. *Marine Chemistry*, *106*(3-4), 530–545. https://doi.org/10.1016/j.marchem.2007.05.006

Polyakov, I. V., Beszczynska, A., Carmack, E. C., Dmitrenko, I. A., Fahrbach, E., Frolov, I. E., et al. (2005). One more step toward a warmer Arctic. *Geophysical Research Letters*, *32*, L17605. https://doi.org/10.1029/2005GL023740

Polyakov, I. V., Pnyushkov, A. V., Alkire, M. B., Ashik, I. M., Baumann, T. M., Carmack, E. C., et al. (2017). Greater role for Atlantic inflows on sea-ice loss in the Eurasian Basin of the Arctic Ocean. *Science*, *356*(6335), 285–291. https://doi.org/10.1126/science.aai8204

Qiao, J., Steier, P., Nielsen, S., Hou, X., Roos, P., & Golser, R. (2017). Anthropogenic ^{236}U in Danish seawater: Global fallout versus reprocessing discharge. *Environmental Science & Technology*, *51*(12), 6867–6876. https://doi.org/10.1021/acs.est.7b00504

Raisbeck, G. M., Yiou, F., Zhou, Z. Q., & Kilius, L. R. (1995). ^{129}I from nuclear fuel reprocessing facilities at Sellafield (U. K.) and La Hague (France): Potential as an oceanographic tracer. *Journal of Marine Systems*, *6*(5-6), 561–570. https://doi.org/10.1016/0924-7963(95)00024-J

Rudels, B. (1995). The thermohaline circulation of the Arctic Ocean and the Greenland Sea. *Philosophical Transactions of the Royal Society A*, *352*, 287–299.

Rudels, B. (2009). Arctic Ocean Circulation. *Encyclopedia of Ocean Sciences*, 211–225. https://doi.org/10.1016/B978-012374473-9.00601-9

Rudels, B., Björk, G., Nilsson, J., Winsor, P., Lake, I., & Nohr, C. (2005). The interaction between waters from the Arctic Ocean and the Nordic Seas north of Fram Strait and along the East Greenland Current: Results from the Arctic Ocean-02 Oden expedition. *Journal of Marine Systems*, *55*(1-2), 1–30. https://doi.org/10.1016/j.jmarsys.2004.06.008

Rudels, B., Jones, E. P., Schauer, U., & Eriksson, P. (2004). Atlantic sources of the Arctic Ocean surface and halocline waters. *Polar Research*, *23*(2), 181–208. https://doi.org/10.3402/polar.v23i2.6278

Rudels, B., Korhonen, M., Schauer, U., Pisarev, S., Rabe, B., & Wisotzki, A. (2015). Circulation and transformation of Atlantic water in the Eurasian Basin and the contribution of the Fram Strait inflow branch to the Arctic Ocean heat budget. *Progress in Oceanography*, *132*, 128–152. https://doi.org/10.1016/j.pocean.2014.04.003

Rudels, B., Meyer, R., Fahrbach, E., Ivanov, V. V., Østerhus, S., Quadfasel, D., et al. (2000). Water mass distribution in Fram Strait and over the Yermak Plateau in summer 1997. *Annales de Geophysique*, *18*(6), 687–705. https://doi.org/10.1007/s00585-000-0687-5

Sakaguchi, A., Kadokura, A., Steier, P., Takahashi, Y., Shizuma, K., Hoshi, M., et al. (2012). Uranium-236 as a new oceanic tracer: A first depth profile in the Japan Sea and comparison with caesium-137. *Earth and Planetary Science Letters*, *333-334*(8), 165–170. https://doi.org/10.1016/j.epsl.2012.04.004

Sakaguchi, A., Kawai, K., Steier, P., Quinto, F., Mino, K., Tomita, J., et al. (2009). First results on ^{236}U levels in global fallout. *Science of the Total Environment*, *407*(14), 4238–4242. https://doi.org/10.1016/j.scitotenv.2009.01.058

Schlichtholz, P., & Houssais, M. N. (2002). An overview of the χ - S correlations in Fram Strait based on the MIZEX 84 data. *Oceanologia*, *44*, 243–272.

Smith, J. N., Ellis, K. M., & Boyd, T. (1999). Circulation features in the central Arctic Ocean revealed by nuclear fuel reprocessing tracers from Scientific Ice Expeditions 1995 and 1996. *Journal of Geophysical Research*, *104*(C12), 29,663–29,677. https://doi.org/10.1029/1999JC900244

Smith, J. N., Ellis, K. M., & Kilius, L. R. (1998). I-129 and Cs-137 tracer measurements in the Arctic Ocean. *Deep-Sea Research Part I: Oceanographic Research Papers*, *45*(6), 959–984. https://doi.org/10.1016/S0967-0637(97)00107-6

Smith, J. N., Jones, E. P., Moran, S. B., Smethie, J. M., & Kieser, W. E. (2005). Iodine 129/CFC 11 transit times for Denmark Strait Overflow Water in the Labrador and Irminger Seas. *Journal of Geophysical Research*, *110*, C05006. https://doi.org/10.1029/2004JC002516

Smith, J. N., McLaughlin, F. A., Smethie, W. M., Moran, S. B., & Lepore, K. (2011). Iodine-129, 137Cs, and CFC-11 tracer transit time distributions in the Arctic Ocean. *Journal of Geophysical Research*, *116*, C04024. https://doi.org/10.1029/2010JC006471

Snyder, G., Aldahan, A., & Possnert, G. (2010). Global distribution and long-term fate of anthropogenic129i in marine and surface water reservoirs. *Geochemistry, Geophysics, Geosystems*, *11*, Q04010. https://doi.org/10.1029/2009GC002910

Stedmon, C. A., Granskog, M. A., & Dodd, P. A. (2015). An approach to estimate the freshwater contribution from glacial melt and precipitation in East Greenland shelf waters using colored dissolved organic matter (CDOM). *Journal of Geophysical Research: Oceans*, *120*, 1107–1117. https://doi.org/10.1002/2014JC010501

Steier, P., Bichler, M., Fifield, L. K., Golser, R., Kutschera, W., Priller, A., et al. (2008). Natural and anthropogenic ^{236}U in environmental samples. *Nuclear Instruments and Methods in Physics Research Section B: Beam Interactions with Materials and Atoms*, *266*(10), 2246–2250. https://doi.org/10.1016/j.nimb.2008.03.002

Tanhua, T., Bulsiewicz, K., & Rhein, M. (2005). Spreading of overflow water from the Greenland to the Labrador Sea. *Geophysical Research Letters*, *32*, L10605. https://doi.org/10.1029/2005GL022700

Vockenhuber, C., Casacuberta, N., Christl, M., & Synal, H. A. (2015). Accelerator mass spectrometry of ^{129}I towards its lower limits. *Nuclear Instruments and Methods in Physics Research Section B: Beam Interactions with Materials and Atoms*, *361*, 445–449. https://doi.org/10.1016/j.nimb.2015.01.061